Development 135, 2227-2238 (2008) doi:10.1242/dev.019802

Control of cell flattening and junctional remodeling during squamous epithelial morphogenesis in *Drosophila*

Karen L. Pope and Tony J. C. Harris*

Diverse types of epithelial morphogenesis drive development. Similar cytoskeletal and cell adhesion machinery orchestrate these changes, but it is unclear how distinct tissue types are produced. Thus, it is important to define and compare different types of morphogenesis. We investigated cell flattening and elongation in the amnioserosa, a squamous epithelium formed at *Drosophila* gastrulation. Amnioserosa cells are initially columnar. Remarkably, they flatten and elongate autonomously by perpendicularly rotating the microtubule cytoskeleton – we call this 'rotary cell elongation'. Apical microtubule protrusion appears to initiate the rotation and microtubule inhibition perturbs the process. F-actin restrains and helps orient the microtubule protrusions. As amnioserosa cells elongate, they maintain their original cell-cell contacts and develop planar polarity. Myosin II localizes to anterior-posterior contacts, while the polarity protein Bazooka (PAR-3) localizes to dorsoventral contacts. Genetic analysis revealed that Myosin II and Bazooka cooperate to properly position adherens junctions. These results identify a specific cellular mechanism of squamous tissue morphogenesis and molecular interactions involved.

KEY WORDS: Cell adhesion, Cell polarity, Cytoskeleton, *Drosophila* embryogenesis, Tissue morphogenesis

INTRODUCTION

Tissue morphogenesis is essential for embryonic development and adult tissue physiology. Epithelia are the most common animal tissue architecture. These sheets of adherent cells form boundaries between body compartments, but are not static. Epithelial remodeling creates and shapes body compartments during embryogenesis, and mediates tissue repair in adults. Tissues can invaginate, converge and extend, flatten or dissociate to properly create and maintain the adult body plan. To understand how different tissues form, we must define how individual cells change their shapes and interactions, and how embryonic signals regulate these changes.

Like isolated cells, cells in tissues can change shape through cytoskeletal rearrangements. For example, actin-myosin contractility drives apical constriction and tissue invagination (Leptin, 1999), or can constrict specific cell-cell contacts driving cell intercalation (Lecuit and Lenne, 2007). Actin-based protrusions drive cell migration during convergent extension (Keller et al., 2003) and wound repair (Van Aelst and Symons, 2002). Microtubule (MT) protrusion has been implicated in cell elongation along the apicobasal axis during tissue invagination (Lee et al., 2007), but MT functions during other tissue rearrangements are unclear.

Cytoskeletal systems integrate with adherens junctions (AJs) to regulate cell-cell interactions and coordinate tissue-wide morphogenesis. AJs form from Cadherin receptors and adaptor proteins β-catenin (Armadillo, Arm) and α-catenin, which associate directly or indirectly with actin and MTs. In *Drosophila*, actin-myosin-AJ links are evident during apical constriction (Dawes-Hoang et al., 2005) and cell intercalation (Bertet et al., 2004). Moreover, interplay between actin and MTs at AJs appears to control symmetric AJ positioning around the apical domain during cell intercalation. These interactions are regulated by the polarity proteins aPKC and PAR-6 (Blankenship et al., 2006; Harris and Peifer, 2007). Additionally, Bazooka (Baz/PAR-3) plays an earlier role in initial apical AJ positioning (Harris and Peifer, 2004; Harris and Peifer, 2005). However, mechanisms that regulate AJ disassembly or assembly as specific cell-cell contacts are lost or expanded remain poorly understood.

To understand core epithelial morphogenesis mechanisms, it is important to study how similar molecular machinery produces different types of epithelia. Epithelial cells can be columnar, cuboidal or squamous. Squamous epithelial cells are flat and elongated in the plane of the epithelial sheet. They are often in stratified epithelia such as the skin, esophagus, trachea, cervix and cornea, where their unique morphology probably provides protective barriers resistant to physical stress. Squamous epithelia can also be monolayers. These are often associated with developmental or tissue remodeling processes. Examples include the trophectoderm of the mammalian embryo (Yamanaka et al., 2006) and the peripodial epithelium of *Drosophila* imaginal disks (Gibson and Schubiger, 2001). Cells also flatten and spread during epiboly (Solnica-Krezel, 2006) and wound healing (Van Aelst and Symons, 2002).

Here, we report cellular and molecular mechanisms that control morphogenesis of the amnioserosa (AS), a squamous epithelial monolayer connected to the main epidermis of the *Drosophila* embryo. The AS plays a central role in guiding major embryo tissue rearrangements, including germband retraction and dorsal closure (Jacinto and Martin, 2001). However, little is known about how the AS first forms. The AS forms during gastrulation from columnar epithelial cells generated at cellularization (the simultaneous formation of the 5000-6000 cells of the first embryonic epithelium). TGF-β signaling specifies AS cells on the dorsal embryo surface (O'Connor et al., 2006), but the cellular mechanisms driving their morphogenesis are unclear. We find that AS cells flatten and elongate autonomously. This elongation occurs through a novel rotation of cellular components converting a columnar morphology into a squamous morphology. Apical MT protrusion appears to initiate the rotation, and actin constrains and

Department of Cell and Systems Biology, University of Toronto, 25 Harbord Street, Toronto, ON, M5S 3G5, Canada.

*Author for correspondence (e-mail: tony.harris@utoronto.ca)

Accepted 2 May 2008

helps orient these MTs. As the cells elongate, they maintain contacts with their original neighbors, and AJs at these contact sites are rapidly remodeled through the coordinated activity of Myosin II and Baz.

MATERIALS AND METHODS

Fly stocks and genetics

FlyBase describes mutations and constructs. GFP lines (all constitutively expressed) were: Tubulin-GFP (Grieder et al., 2000), Moesin ABD-GFP (Kiehart et al., 2000), YFP-endoplasmic reticulum (ER) targeting sequence [Bloomington Drosophila Stock Center (BDSC)], DE-Cad-GFP (Oda and Tsukita, 2001), Spaghetti squash (Sqh)-GFP (Royou et al., 2002), EB1-GFP [a gift from H. Ohkura (Edinburgh University, UK)] and Baz-GFP (Flytrap). Arm-CFP generated as Arm-GFP has been described previously (McCartney et al., 2001). *arm*^{XP33} maternal-zygotic mutants were made as before (Harris and Peifer, 2004). *baz*^{Xi106} mutants were a gift from A. Wodarz (Göttingen University, Germany). *bcd*^{E1} *nos*^{L7} *tsl*^{146} mutants were a gift from E. Wieschaus (Princeton, NJ, USA). *dl*^{1}, *zen*^{7} and *zip*^{1} mutants were from BDSC. The wild type used was *yellow white*.

Embryo staining and treatment

For tubulin and phalloidin staining, embryos were fixed for 10 minutes in 1:1 10% formaldehyde/PBS:heptane and were de-vitellinized by hand peeling. For other staining, embryos were fixed for 20 minutes in 1:1 3.7% formaldehyde/PBS:heptane and were de-vitellinized with methanol. Blocking and staining was carried out in PBS/1% goat serum/0.1% Triton X-100. Antibodies used were: mouse Dlg [1:100; Developmental Studies Hybridoma Bank (DSHB)], γ-tubulin (1:350; Sigma), acetylated tubulin (1:350; Sigma) and tubulin (1:100; DSHB); rabbit Baz (1:350) and GFP (1:2000; Abcam); and rat DE-Cad [1:100 (Oda et al., 1994)]. F-actin staining was carried out with phalloidin-Alexa488 (Invitrogen). Colchicine and cytochalasin D treatments were carried out as previously described (Harris and Peifer, 2005).

Image acquisition, quantification and manipulation

Fixed embryos were mounted in Aqua Polymount (Polysciences) and were imaged using a 510 confocal microscope (Carl Zeiss) at room temperature. Lenses used were 40× (Plan-NeoFluor; NA 1.3) and 63× (Plan-Apochromat; NA 1.4) objectives. Images were analyzed using LSM 510 AIM software. Secondary Abs were Alexa488, 546 and 647 (Invitrogen). Image deconvolution and projections were carried out by Volocity software (Improvision). Fluorescence intensity measurement was made using Image J (NIH). Unless otherwise noted, input levels were adjusted by Adobe Photoshop for the main signal range to span full output grayscale. Image re-sizing was carried out using bicubic interpolation (minimal change at normal magnifications).

Time-lapse microscopy

Dechorionated embryos were mounted in halocarbon oil (series 700; Halocarbon Products) on petriPERM dishes (Sigma). Analysis was carried out using a Quorum spinning disk confocal microscope (Quorum Technologies) at room temperature with 40× (Plan-NeoFluor; NA 1.3) and 63× (Plan-Apochromat; NA 1.4) objectives. Images were captured in 300 nm *z*-steps using a piezo top plate and Hamamatsu EM CCD camera linked to Volocity software.

RESULTS

Amnioserosa morphogenesis involves dramatic cell shape change

Five major morphogenetic movements occur at *Drosophila* gastrulation (Leptin, 1999). First, the cephalic furrow separates head and body, and the ventral furrow internalizes the mesoderm. Second, the posterior midgut invaginates from the posterior pole, and the lateral germband undergoes convergent extension along the anteroposterior (AP) axis (germband extension). Simultaneously, the AS forms on the dorsal surface. The AS initially extends along the DV axis, filling space left by the germband (Fig. 1A, the AS is bracketed). Next, the AS spreads posteriorly, filling space between the ventral and dorsal halves of the extended germband (Fig. 1B,C, the AS is bracketed).

To overview AS cell shape changes, we examined AJ, MT and actin localization in fixed tissue. After cellularization, AS cells, like other blastoderm cells, are hexagonal and columnar with DE-Cadherin (DE-Cad; Cad in figures) in spot junctions around the cell apex (Fig. 1D) (Tepass and Hartenstein, 1994). The cells have apical diameters of 5.1±1.0 μm (100 cells from 10 embryos) and depths of 18.9±2.9 μm (60 cells from 12 embryos) (Fig. 1D,M, two cells outlined, inset shows cell height). Lateral MT bundles run from the level of AJs basally (Harris and Peifer, 2007) (Fig. 1D,E). Actin partially colocalizes with AJs (Pilot et al., 2006) (Fig. 1F) but is also in apical surface microvilli (Grevengoed et al., 2003) and lateral (data not shown). After germband extension, AS cells are fully elongated, with average lengths of 52.7±12.7 μm, widths of 4.9±1.6 μm (32 cells from four embryos) and depths of 4.27±0.75 μm (21 positions from 11 embryos at the cell centre – the cells taper at both ends) (Fig. 1J,M, two cells are outlined, inset shows cell height). AJs form more continuous belt junctions during this transition (Fig. 1G,J) (Tepass and Hartenstein, 1994), and remain around the full cell circumference (Fig. 1G,J). MT bundles reorganize to run along the axis of cell elongation (Fig. 1H,K, arrows). Actin localizes around the full cell circumference (Fig. 1I,L). Overall, AS cell elongation requires AJ and actin reorganization for continual positioning around the growing apical circumference, and MT reorganization from a series of bundles along the apicobasal axis to a perpendicular series of bundles along the long axis of the flattened cell.

Autonomy of the amnioserosa cell shape change

Because AS morphogenesis coincides closely with germband extension and ventral furrow formation, we wondered which elements of AS morphogenesis are cell autonomous (i.e. orchestrated by changes within AS cells themselves), and which might involve surrounding tissues. Thus, we examined mutants affecting each tissue. To assess whether germband extension and ventral furrow formation are sufficient for elongating dorsal cells, we analyzed *zerknüllt* (*zen*) zygotic mutants in which AS differentiation is blocked but ventral furrow formation and germband extension occur (Arora and Nusslein-Volhard, 1992). Stage 7-10 *zen* mutant embryos displayed no dorsal cell elongation relative to *zen* mutant germband cells (Fig. 1N, dorsal cells bracketed; Fig. 1T,U show higher magnification and cell length quantification). However, the ventral midline of the extended germband was observed below the non-elongated dorsal cells in 3D projections (Fig. 1O, arrow) – the *zen* mutant germband has previously been shown to extend beneath the non-differentiated dorsal cells (Arora and Nusslein-Volhard, 1992). Thus, ventral furrow formation and germband extension are not sufficient for changing dorsal cell shape, indicating that amnioserosa specification is either instructive or permissive for amnioserosa morphogenesis.

To test whether amnioserosa specification is instructive, we examined *arm* maternal/zygotic mutants. These form the first embryonic epithelium with apicobasal polarity and proper embryonic axes, but at gastrulation epithelial structure is disrupted and ventral furrow formation and germband extension fail (Cox et al., 1996; Harris and Peifer, 2004). In gastrulating *arm* mutants, we observed elongating dorsal cells (Fig. 1P, brackets; ventral and ventrolateral markers identified the dorsal surface). In stage 9-11 *arm* mutants, highly elongated dorsal cells were present, but were

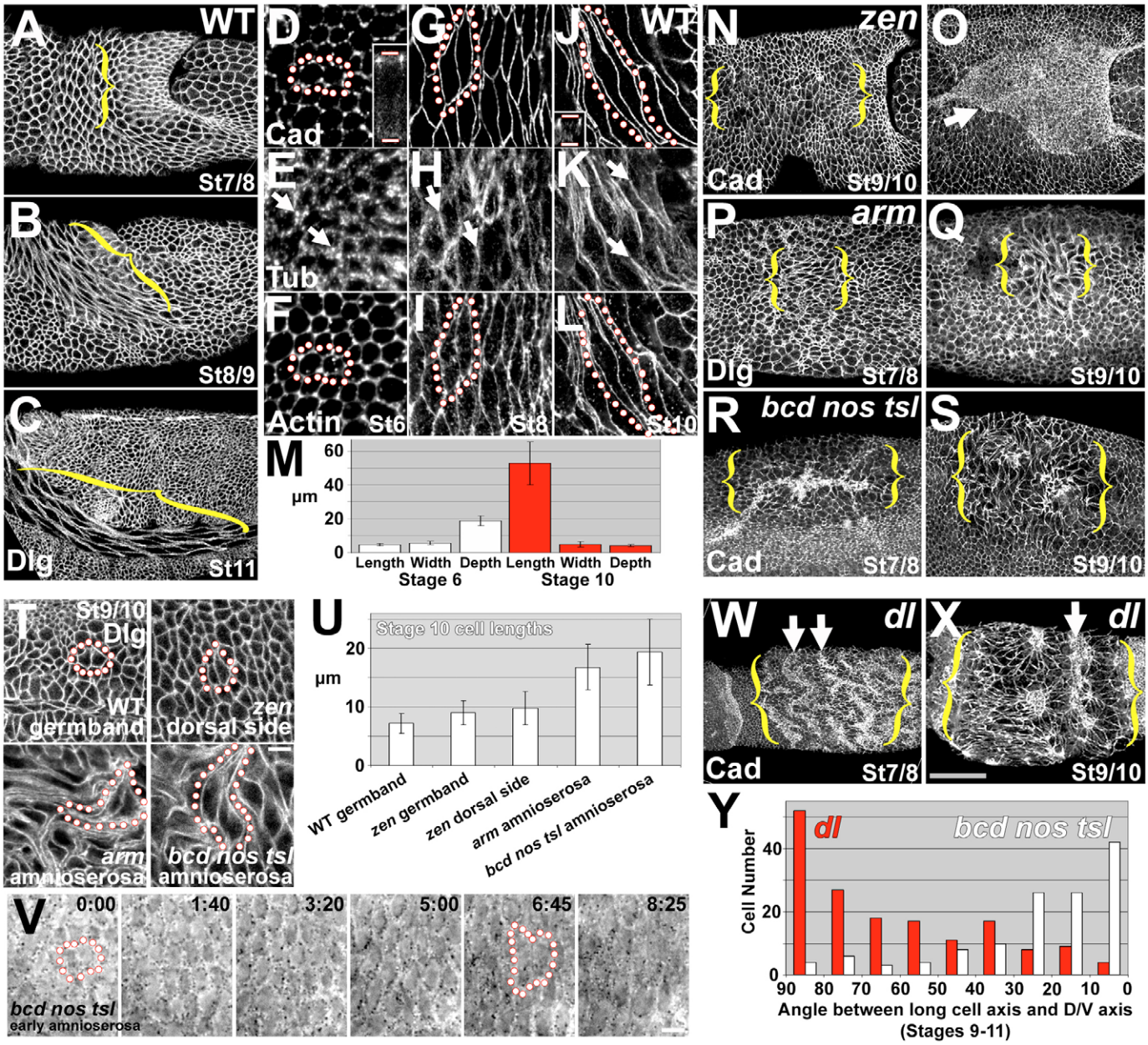

Fig. 1. The autonomy of amnioserosa morphogenesis. (**A-L**) Wild-type embryos. Stage 7-8 (A) and stage 8-9 (B). AS is bracketed. (C) Stage 10-11. Fully extended AS (bracketed) is present between folded germband. (D-L) Embryo surface views at the level of AJs. (D-F) Stage 6. (D) DE-Cadherin. Two hexagonal AS cells are outlined. Inset shows a cross-section. (E) Lateral MT bundles in cross-section (arrows). (F) F-actin, AS cells are outlined. (G-I) Stage 8. (G) DE-Cadherin. Two AS cells elongating along DV axis are outlined. (H) MTs along cell elongation axis (arrows). (I) Actin, AS cells are outlined. (J-L) Stage 10. (J) DE-Cadherin. Two fully elongated AS cells are outlined. Inset shows a cross-section. (K) MT bundles along cell elongation axis (arrows). (L) Actin, AS cells are outlined. (**M**) Cell dimensions pre/post-elongation. (**N**,**O**) Stage 9-10 *zen* mutant. (N) Non-elongated dorsal cells are bracketed. (O) Projection. The germband ventral midline (arrow) extended beneath dorsal surface. (**P**,**Q**) $arm^{m/z}$ mutant. Elongated dorsal cells are bracketed. (P) After cellularization. (Q) Stage 9-10. (**R**,**S**) *bcd nos tsl* mutant. Elongated dorsal cells are bracketed. (R) Stage 7-8. (S) Stage 9-10. (**T**) Higher magnification wild-type, *zen* mutant, $arm^{m/z}$ mutant and *bcd nos tsl* mutant cells. Two cells are outlined in each. (**U**) Quantification of stage 10 wild-type, *zen* mutant, $arm^{m/z}$ mutant and *bcd nos tsl* mutant cell lengths. (**V**) Bright-field timelapse imaging. Early *bcd nos tsl* mutant AS morphogenesis. Two cells are outlined. (**W**,**X**) *dl* mutant. DE-Cadherin. AS is bracketed. Ectopic furrows are indicated by arrows. (W) Stage 7-8. (X) Stage 9-10. (**Y**) Stage 9-11 AS cell orientations. *bcd nos tsl* mutants, white; *dl* mutants, red. White scale bar, 5 µm; gray scale bar, 50 µm.

restricted to a dorsal patch in which they formed abnormal swirls of cells (Fig. 1Q, brackets; Fig. 1T,U show higher magnification and cell length quantification). Thus, individual AS cells can elongate without ventral furrow formation and germband extension.

Finally, we examined mutants affecting AP and DV embryo patterning. *bicoid*, *nanos* and *torso-like* (*bcd nos tsl*) maternal mutants form the first embryonic epithelium and form a ventral furrow, but germband extension is blocked because A-P patterning is disrupted (Irvine and Wieschaus, 1994). In

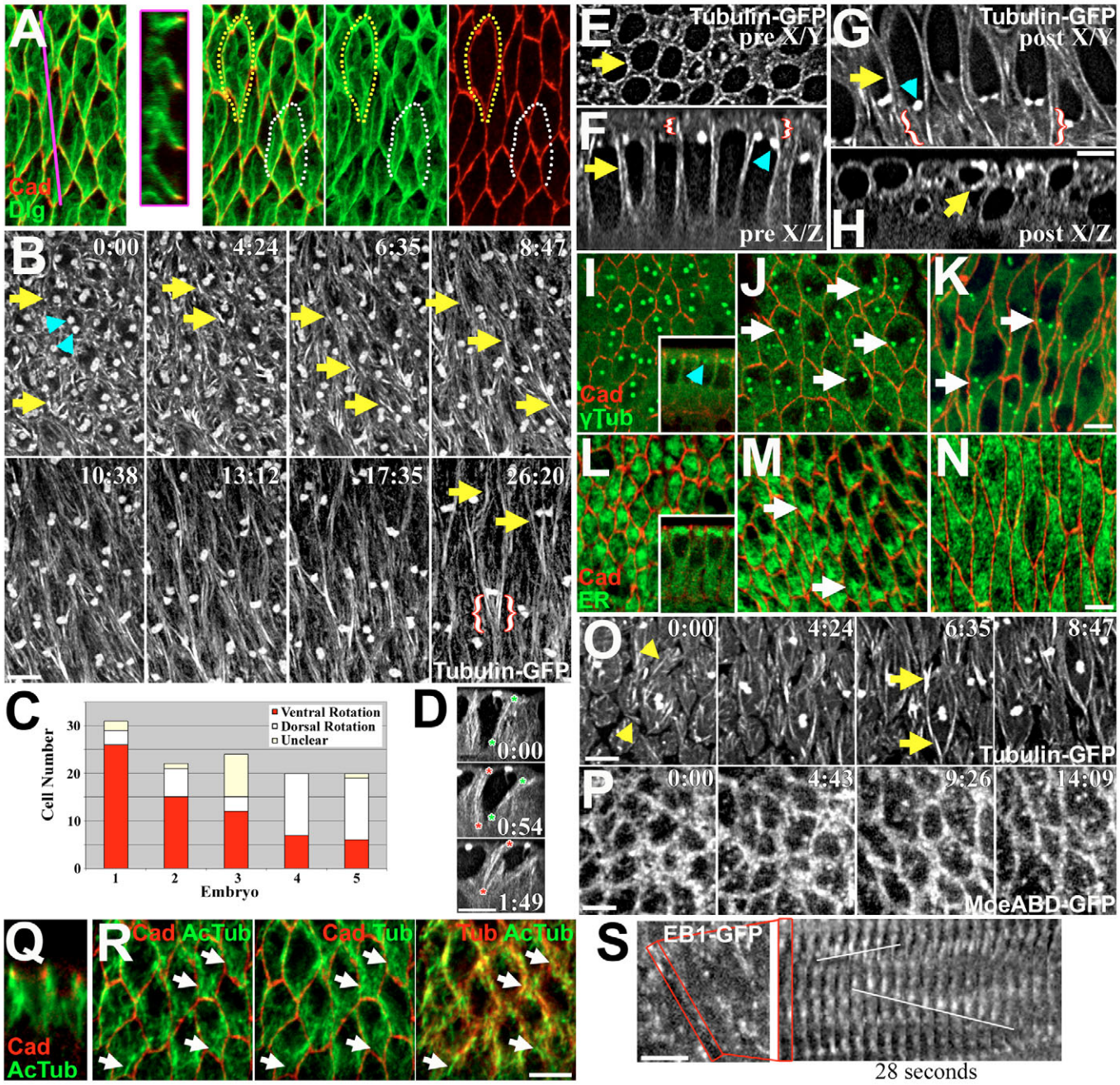

Fig. 2. Amnioserosa cell elongation involves rotation of the MT cytoskeleton. (**A**) Stage 7-8 AS 3D projections. DE-Cad (red). Dlg (green). Purple line and box show a cross-section. Basolateral membranes of two cells are outlined. (**B**) Three-dimensional projections of Tubulin-GFP as live AS cells elongate. Smooth MT rotation from apical basal axis (0:00, arrows show bundle end-on views) to cell elongation axis (4:24-26:20, arrows). Centrosomes are detected (arrowheads). Gamma adjustments are made to visualize all MTs. (**C**) Rotation direction quantification. (**D**) Single rotating cell. Side view. Rotating MT bundles (asterisks). (**E**,**F**) Pre-elongation live embryo in single plane surface view (E) or in cross section (F). Tubulin-GFP staining. MT bundles are in cross-section (E, arrow) or seen longitudinally (F, arrow). Centrosomes (F, arrowheads) above elongated nuclei (dark ovals). MTs above centrosomes are bracketed (F). (**G**,**H**) During elongation live embryo in single plane surface view (G) or in cross section (H). Tubulin-GFP staining. MT bundles are seen longitudinally (G, arrow) or in cross-section (H, arrow). Centrosomes (G, arrowhead) at one end of elongated nuclei (G, dark ovals). MT extension past centrosomes (G, brackets). (**I-K**) DE-Cad (red), centrosomes (γtubulin, green). (I) Pre-elongation, surface view. Centrosomes (arrowhead) above nuclei (inset, cross-section). (J,K) During elongation. Centrosomes at one end of nuclei (arrows, dark circles). (**L-N**) DE-Cad (red), YFP-ER targeting sequence (green). (L) Pre-elongation, surface view. ER bulk above nuclei (inset, cross-section). (M) During elongation the bulk of the ER is at one cell end (arrows) but evens out later (N). (**O**,**P**) Projections. AS cells are at early elongation. Apical Tubulin-GFP (O) and Moesin-ABD-GFP (P). (**Q**) Pre-elongation, cross-section. DE-Cad, red; acetylated tubulin, green. (**R**) Elongating, surface view. DE-Cad, red; acetylated tubulin, green; tubulin, green/red. Acetylated microtubules along cell elongation axis (arrows). (**S**) During elongation, surface view. EB1-GFP staining. Kymogram of box of one cell side. White lines indicate two EB-1 complexes. Scale bars: 5 μm.

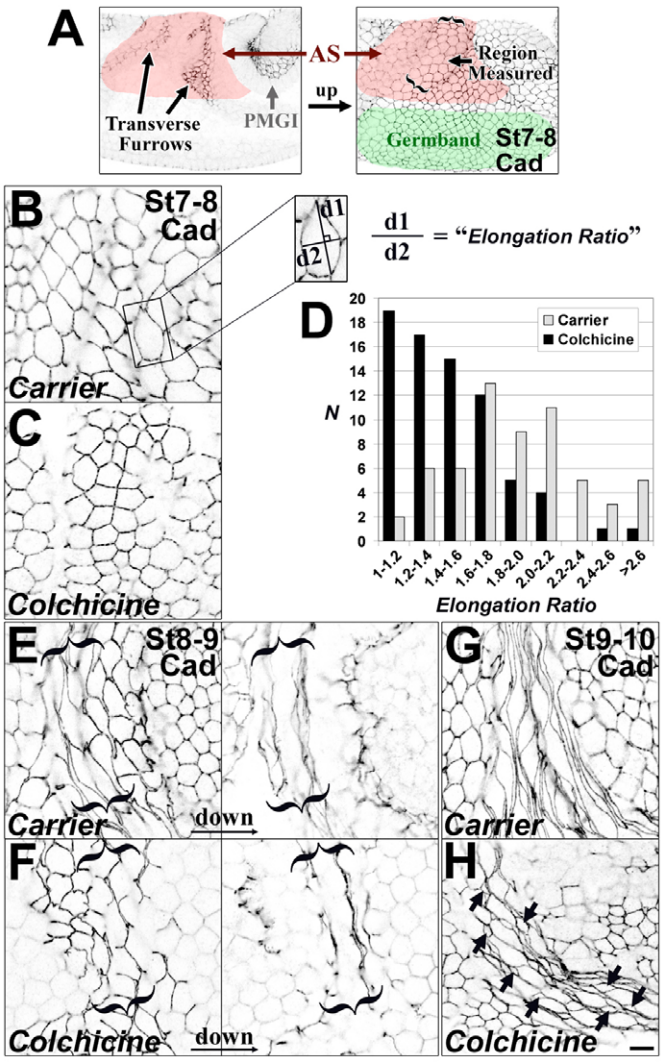

Fig. 3. MTs function in initiating amnioserosa cell elongation. DE-Cadherin marks cell outlines. (**A**) Embryo stage/region measured. Transverse furrows below surface AS. PMGI, posterior midgut invagination. (B,E,G) 30-minute treatment with carrier. (C,F,H) 30-minute treatment with colchicine. (**B**,**C**) Stage 7-8 [transverse furrow cells columnar (not shown)]. Initial AS cell elongation occurs with carrier (B) but not with colchicine (C). (**D**) Cell elongation quantification. (**E**,**F**) Stage 8-9. Elongated surface cells with carrier (E), but not with colchicine (F). Elongated cells in transverse furrows in both (bracketed). (**G**,**H**) Stage 9-10. The full AS cell length is surface-exposed with carrier (G). Elongated cells show less surface exposure with colchicine (H, arrows). Scale bar: 5 μm.

gastrulating and stage 9-11 *bcd nos tsl* mutants, dorsal cells elongated individually but the tissue remained in a dorsal patch similar to *arm* mutants (Fig. 1R,S, brackets; Fig. 1T,U show higher magnification and cell length quantification). AS patches were significantly larger in stage 9-11 *bcd nos tsl* mutants versus stage 9-11 *arm* mutants (130.4±19 μm versus 60.2±21.7 μm lengths, n>10, P<0.001, t-test), suggesting defects in forming/maintaining full patch size without AJs. Intriguingly, stage 9-10 *bcd nos tsl* mutant AS cells preferentially elongated along the DV axis (Fig. 1S, quantified in 1Y), although there was more tissue disorganization versus wild type (Fig. 1B,C). Live bright-field imaging of *bcd nos tsl* mutants revealed initial cell elongation along the DV axis (Fig. 1V) and later disorganization. We suspected that DV patterning might initially orient the cells, and thus analyzed *dl* mutants that fail to form ventral tissue and instead form a ring of AS around the full DV axis at the centre of the embryo (Ray et al., 1991) (Fig. 1W,X; bracketed). Here, AS cells also elongated but reoriented along the AP axis (Fig. 1W,X, quantified in Fig. 1Y) towards ectopic furrows (Fig. 1W,X, arrows). Thus, AS cells can elongate with disruption of either germband extension or the ventral furrow in *bcd nos tsl* mutants and *dl* mutants, respectively, further confirming the autonomy of individual AS cell shape change. However, mechanisms involving outside tissues may orient the cells.

Amnioserosa cell elongation involves a 90° rotation of the MT network

To determine how AS cells change shape, we began with 3D imaging of fixed stage 7-8 wild-type embryos stained for DE-Cad to mark apical circumferences and Dlg to mark basolateral membranes. Cross-sections revealed lateral membranes slanted into the cell elongation axis, with either both sides or mainly one cell side slanted (Fig. 2A; purple line and box). Three-dimensional projections of the embryo surface also revealed cells with both basolateral membranes slanted (Fig. 2A, yellow dots) and cells with mainly one lateral membrane slanted (Fig. 2A, white dots). This suggested AS cell elongation occurred through rotation of cell contents rather than simple symmetric cell flattening.

To further evaluate the cell rotation, we examined the full MT network by 3D timelapse imaging of Tubulin-GFP. First, we analyzed 3D projection embryo surface views (see Movie 1 in the supplementary material). Before elongation, lateral MT bundles run along the apicobasal axis and are seen end-on (Fig. 2B, 0:00, arrows), with minimal links to the centrosomes (Fig. 2B, 0:00, arrowheads, above nuclei). Then, lateral bundles smoothly rotate into the axis of cell elongation, progressively revealing the long axis of the bundles in embryo surface views (Fig. 2B, 4:24-26:20, arrows). Notably, the cells could rotate in either direction along the axis of tissue extension (dorsally or ventrally) (Fig. 2C). These 3D projection analyses allowed detection of the overall rotation of the MT arrays, but the overlapping of structures with this imaging hindered analysis of individual elements of the arrays.

To clearly view individual elements of the arrays, we analyzed single sections from our 3D imaging. We viewed cells in cross-section and found individual lateral MT bundles progressively rotating from the apicobasal axis to the axis of tissue extension (Fig. 2D, two bundles marked individually with red and green asterisks). We also evaluated the rotation of the full MT network. Before elongation, embryo surface views revealed a ring of MT bundles in cross-section per cell (Fig. 2E, arrows, section at top of nuclei), whereas embryo cross-section views revealed long axes of the bundles (Fig. 2F, arrows). With cell elongation, embryo surface views revealed long axes of the bundles (Fig. 2G, arrows), whereas embryo cross-section views reveal a ring of MT bundles in cross-section per cell (Fig. 2H, arrows, section at end of nuclei). Before rotation, full MT arrays were 17.7±3.0 μm long, equaling cell depths. After 10 minutes rotation, the MT arrays had similar lengths (18.3±4.9 μm) but cell depths were significantly reduced (12.8±3.6 μm, P<0.001, t-test, 15 arrays from three embryos). Thus, the MT network appears to rotate as a unit as the cells flatten.

With rotation of the MT array, organelles initially polarized along the apicobasal axis should become planar polarized. Thus, we examined the positioning of the nucleus, centrosomes, ER and Golgi. At the end of cellularization nuclei are elongated along the apicobasal axis (Fig. 2F, seen by Tubulin-GFP nuclear exclusion), and two centrosomes localize above each nucleus (Fig. 2F,I, arrowheads, inset). With cell elongation, the nucleus long axis turns perpendicularly into the DV axis of the embryo (Fig. 2G), and the two centrosomes become positioned to the dorsal or ventral end of the cell (Fig. 2G, arrowheads; in fixed tissues in Fig. 2J,K, arrows). A bulk of ER is also above the nuclei following cellularization (Fig. 2L, inset), whereas the Golgi is non-polarized (not shown). During initial AS cell elongation, the ER is also positioned at ventral or dorsal ends of the cells (Fig. 2M, arrows), but then becomes non-polarized (Fig. 2N). These results indicate that the centrosomes, nuclei and ER also rotate as AS cells elongate. The apicobasal axis of the main MT network appears to rotate 90° to extend along the DV axis of the embryo: we call this 'rotary cell elongation'.

Amnioserosa cell elongation is microtubule dependent

We hypothesized that MTs actively drive AS cell elongation. As the cells elongated non-centrosomal MT bundles extended past the centrosomes in the direction of cell elongation (compare Fig. 2F with 2G, brackets; Fig. 2B, 26:20, brackets). We evaluated MT organization in 3D image projections of the apical region to assess how these protruding MTs develop. Immediately before cell elongation, we observed apical MTs oriented perpendicularly to lateral MT bundles but without specific AP or DV directionality (Fig. 2O, 0:00, arrowheads). As the cells elongated, these apical MTs then extended preferentially along the DV axis (Fig. 2O, arrows). By contrast, cortical actin is relatively evenly distributed during the process (Fig. 2P).

To understand how the MTs protrude, we probed them for acetylated tubulin to detect older MTs, and imaged EB1-GFP to detect new MT growth. Lateral bundles present before elongation contained acetylated MTs (Fig. 2Q). During AS cell elongation, MT bundles running across the apical domain also contained acetylated MTs (Fig. 2R, arrows), but double staining for total tubulin also suggested the presence of non-acetylated MTs (Fig. 2R). Indeed, EB1-GFP imaging revealed puncta moving in both directions along the long axis of extending AS apical domains (kymogram in Fig. 2S; see Movie 2 in the supplementary material). Thus, apical MT bundles appear to protrude through rotational re-positioning of older lateral MTs and new bi-directional MT growth.

To test MT function during AS cell elongation, we treated embryos for 30 minutes with colchicine, fixed immediately and stained for DE-Cad as a marker for cell shape. During initial cell elongation (cells were still columnar in transverse furrows that form across the early AS, Fig. 3A), the colchicine treatment reduced elongation of the apical domain (Fig. 3C) versus control (Fig. 3B). Elongation was quantified by dividing the longest cell axis by the cell width at half the long axis (Fig. 3D, inset). At this stage, the control ratio was 1.92±0.53 (60 cells from six embryos) and colchicine treatment produced a significantly lower ratio of 1.46±0.34 (74 cells from nine embryos) ($P<0.001$, *t*-test) (Fig. 3D). Thus, MTs function in initiating AS cell elongation.

To test whether MTs maintain cell elongation, we examined later stages. In stage 8-9 control embryos, elongated cells were between two regions of less elongated cells, and in AS transverse furrows (Fig. 3E). In stage 8-9 colchicine-treated embryos, elongated cells lost their embryo surface position, but were in transverse furrows beneath the less elongated cells (Fig. 3F). In stage 9-10 control embryos, elongated cells were arranged in parallel over the embryo surface (Fig. 3G). In stage 9-10 colchicine-treated embryos, AS cells were elongated but had smaller surface-exposed regions (Fig. 3H). Thus, MTs appear to affect cell-cell interactions at later stages, but may not be needed for maintaining AS cell elongation.

Actin restrains microtubule protrusion during cell elongation

As actin often controls cell shape, we examined its role in early AS cell shape change. We treated embryos for 30 minutes with cytochalasin D, fixed immediately and stained for DE-Cad. At stage 7-8, initial cell elongation was evident in carrier controls (Fig. 4A,C). Remarkably, cytochalasin D treatment produced excessive AS cell protrusion (Fig. 4B,D, arrows) – cells extended single abnormally long protrusions with improper orientation (Fig. 4D,H; seen in 13/13 embryos, four experiments). DE-Cad often clustered at these protrusions (Fig. 4D,H), contrasting its normal symmetric distribution (Fig. 4C,G). Germband cells displayed less severe cell shape change with the treatment (Fig. 4A,B), whereas ventral furrow cells rounded up but did not display abnormal cell protrusions (not shown). Phalloidin staining indicated residual filamentous actin after the treatment (not shown). Thus, AS cells are uniquely sensitive to partial actin disruption at this stage, producing abnormally long cell protrusions.

As MTs function in normal AS cell elongation, we hypothesized that MTs might be responsible for the abnormal apical protrusions with actin disruption. Thus, we disrupted actin and MTs simultaneously. This suppressed cell protrusions otherwise produced by actin disruption, and restored AJ symmetry [double treatment in Fig. 4F is more similar to colchicine treatment alone (Fig. 4E) than to cytochalasin D treatment alone (Fig. 4D); clear suppression in 10/12 embryos, two experiments]. Thus, actin may normally counteract MTs during early AS cell elongation.

Weakening actin triggers MT-based flattening and elongation of normally columnar epithelial cells

Although cytochalasin D has a relatively specific effect on AS cells during gastrulation, it induced dramatic reorganization of stage 9-11 germband cells. DE-Cad-positive apical domains were abnormally extended and clustered, forming large rosettes of cells (Fig. 4J, bracketed; seen in 31/31 embryos, five experiments; control in Fig. 4I). The cells appeared to re-orient towards tissue regions that normally have greater apical constriction (Fig. 4I, arrow), and lateral cell surfaces became exposed to the embryo surface [observed with Dlg staining (not shown), and MT staining (Fig. 4L)]. With actin disruption, these cells appeared to rotate perpendicularly relative to their original axis but did not distribute AJs around their subsequently surface-exposed perimeter.

As this abnormal cell shape change resembled normal AS cell shape change, we suspected that MTs might be involved. Thus, we disrupted actin and MTs simultaneously. This suppressed the cytochalasin D-induced germband cell shape change (Fig. 4K; clear suppression in 25/26 embryos, three experiments). Moreover, with actin disruption alone, MTs protruded into the abnormally extended apical domains of the germband cells (Fig. 4L, an arrow marks an apical protrusion and a broken line indicates the surface-exposed lateral region of the cell). Live DE-Cad-GFP imaging after cytochalasin D treatment revealed minimal movement of the

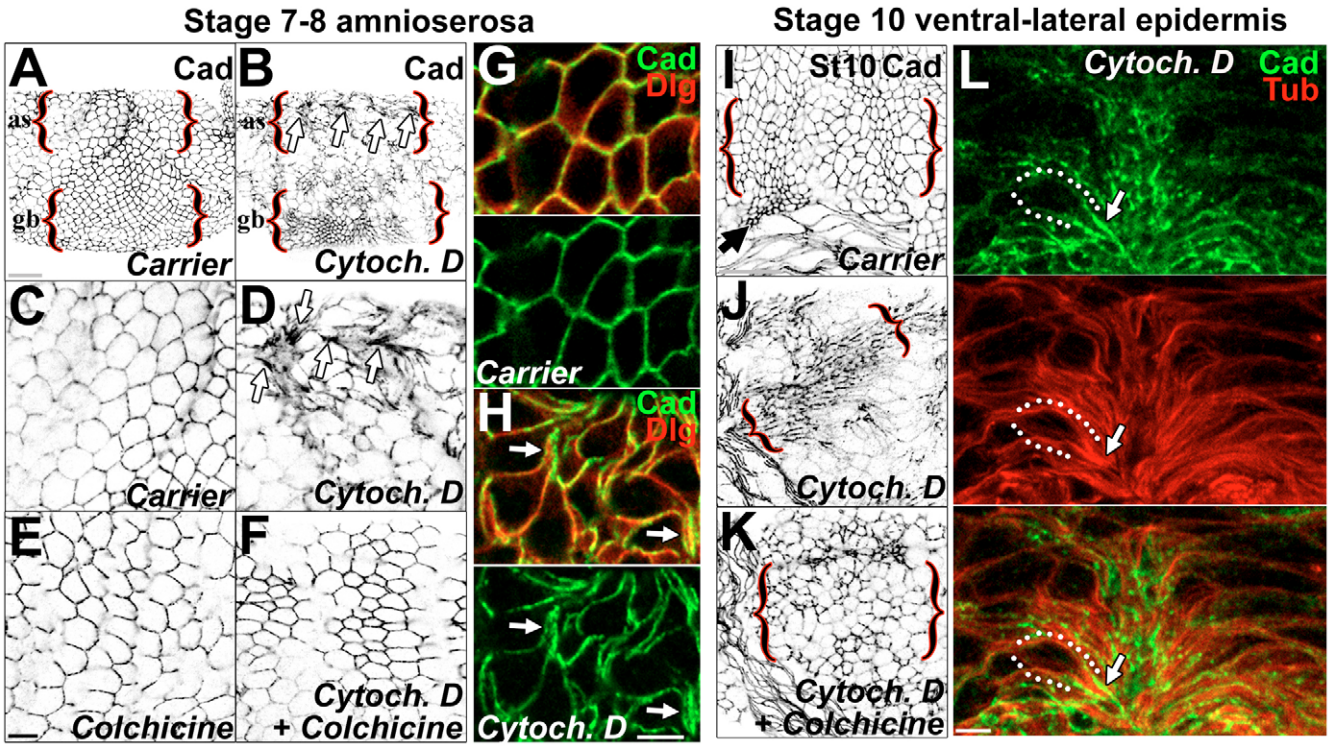

Fig. 4. Actin inhibits apical MT protrusion. (**A-F**) Stage 7-8. DE-Cadherin marks cell outlines. (A) Carrier. (B) Cytochalasin D. AS apical cell protrusions (bracketed, arrows). (C,D) AS cells in A,B are magnified. (E) Colchicine alone. (F) Simultaneous colchicine and cytochalasin D. (**G**,**H**) Stage 7-8 AS cells. DE-Cad (green). Dlg (red). (G) Carrier. (H) Cytochalasin D. (**I-L**) Stage 10 germband. (I-K) DE-Cad. (I) Carrier. Normal DE-Cad (bracketed). Normal contractile region (arrow). (J) Cytochalasin D. Clustered DE-Cad-positive protrusions (bracketed). (K) Simultaneous colchicine and cytochalasin D. Protrusions are suppressed (bracketed). (L) Cytochalasin D. MTs (red) in DE-Cad (green)-positive protrusions (arrow). Lateral MTs embryo surface-exposed (outlined). White/black scale bars 5 μm; gray bars, 25 μm.

extended apical domains (data not shown), suggesting that they remain adherent to each other. Together, these results indicate that actin inhibits apical MT protrusion to maintain columnar versus elongated epithelial cell shape in the later germband. This suggests that normal, MT-driven AS cell elongation involves regulated reduction of apical actin activity.

Amnioserosa tissue extension occurs without cell intercalation but involves two types of AJ remodeling

To investigate how individual AS cell elongation translates into polarized tissue extension, we examined cell-cell interactions by performing 3D timelapse imaging of DE-Cad-GFP. In projections, all cell-cell contacts were seen. One hundred out of 100 DV contacts and 68/68 AP contacts present at the start of AS tissue extension were maintained during the process (Fig. 5A, see Movie 3 in the supplementary material). Thus, AS tissue extension occurs without cell intercalation. Cells maintain contacts as they elongate and two contact types develop: highly elongating AP contacts and lesser elongating DV contacts.

Next, we examined AJ changes at both AP and DV contacts. Remarkably, the length of AP contacts doubled in 5-10 minutes and quadrupled in 10-20 minutes [Fig. 5B; both DE-Cad-GFP and Moesin actin-binding-domain (ABD) GFP expressing embryos analyzed]. DE-Cad-GFP levels per membrane area at AP contacts were approximately half those in the same area at DV contacts at fourfold cell elongation (Fig. 5C), suggesting AJ redistribution along AP contacts. However, AJs were not static at DV contacts. In 3D projections, DV contacts displayed dynamic looping of DE-Cad-GFP, suggesting AJ remodeling at these sites as well (Fig. 5D, arrows; Arm-CFP loops, Fig. 6G, arrows). Thus, the translation of rotary cell elongation into tissue extension involves planar polarized AJ remodeling at both AP and DV contacts.

Myosin II and Bazooka show transient opposite planar polarization in the amnioserosa

Planar polarized junctional remodeling also occurs in the germband. Here, Myosin II is enriched at AP cell contacts, and the polarity and AJ regulator Baz is enriched at DV cell contacts (Zallen and Wieschaus, 2004). To determine whether AS cells share this organization, we localized Myosin II and Baz. Before AS cell elongation, Myosin II localized relatively symmetrically, with AJs and apical to AJs (Fig. 6A, apical surface bracketed), and Baz also localized relatively symmetrically (Fig. 6D). As AS cells elongated, Myosin II became enriched along AP cell contacts (Fig. 6B, arrows; see Movie 4 in the supplementary material), versus DV contacts, and also localized to two ends of AP contacts (Fig. 6B, yellow arrowheads), suggesting loss from the contact length. Baz displayed the reciprocal pattern, with enrichment along DV cell contacts (Fig. 6E, arrows) versus AP contacts [also seen live with Baz-GFP (see Movie 5 in the supplementary material)]. Intriguingly, double live imaging revealed D/V Baz-GFP partly colocalizing with Arm-CFP loops at this stage (Fig. 6G, arrows). With full AS cell elongation, both Myosin II and Baz were lost from the cell cortex, versus germband cells (Fig. 6C,F).

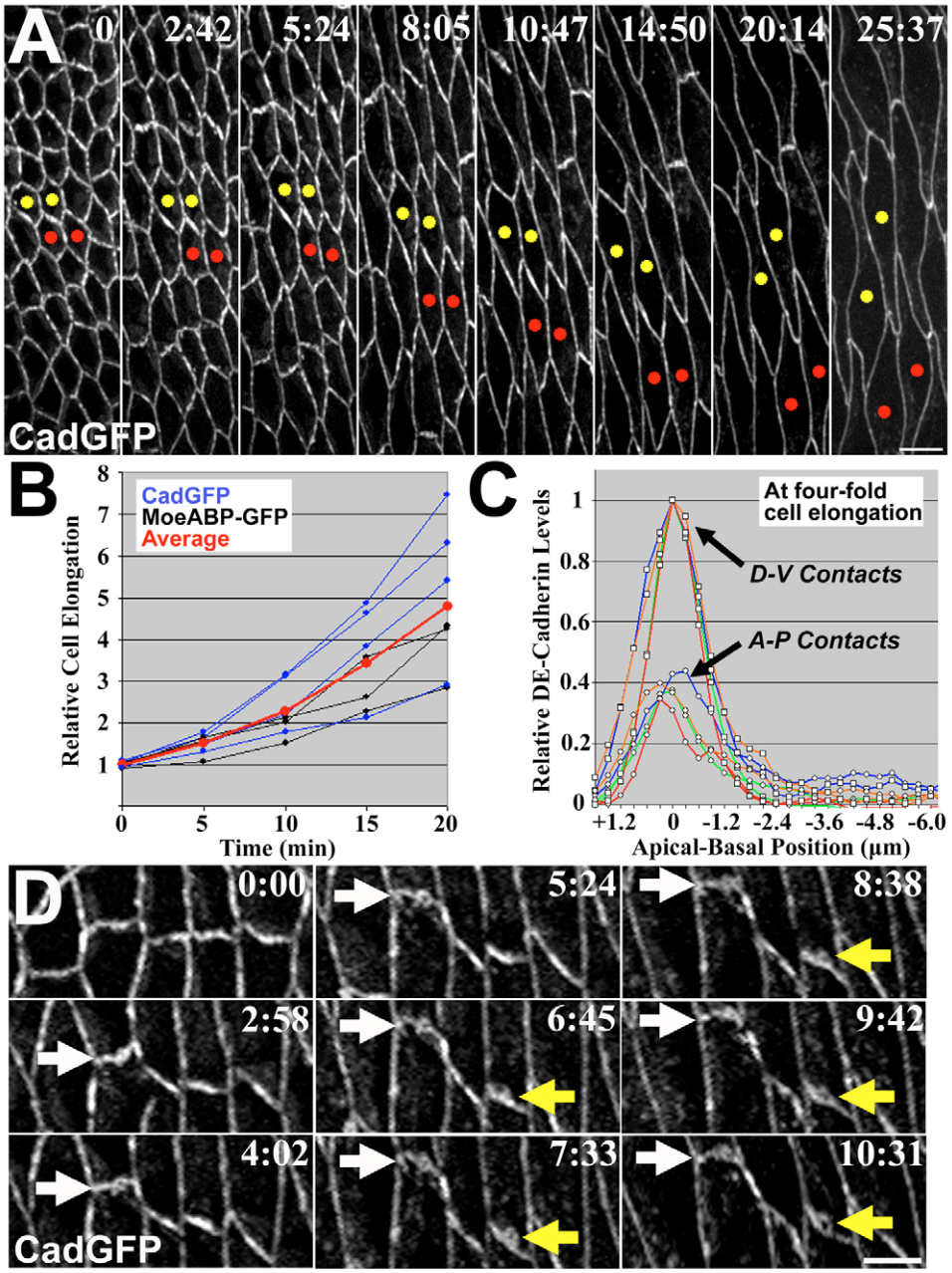

Fig. 5. Amnioserosa extension through rapid cell elongation without intercalation. (**A**) Three-dimensional projections. DE-Cad-GFP. AS cell elongation. Four marked neighboring cells retain contacts. (**B**) Initial AS cell elongation rates. Blue lines indicate average elongation rate for five cells, DE-Cad-GFP embryos. Black lines indicate average elongation rate for five cells, Moesin ABD-GFP embryos. Red line indicates the all embryo average. (**C**) DE-Cadherin-GFP level quantification through confocal stacks. Background-corrected AP and DV contact values normalized to DV contact value for each cell. Five cell averages per embryo are shown (four embryos, different colors). Squares, DV contacts; circles, AP contacts (arrows). (**D**) Three-dimensional projections. DV contacts (white arrows), DE-Cad-GFP looping (yellow arrows). Scale bars: 5 µm.

Myosin II and Bazooka synergize to regulate amnioserosa AJ remodeling

To assess whether Myosin II and Baz affect AJ localization during AS cell elongation, we examined DE-Cad localization in zygotic mutants for *zipper* (*zip*), the Myosin II heavy chain gene and *baz*. DE-Cad appeared normal in stage 8-10 AS cells in both homozygous zygotic *zip* mutants and hemizygous zygotic *baz* mutants (*baz* is X-linked) (data not shown). However, abnormal AS AJ clustering occurred in hemizygous zygotic *baz* mutants derived from females carrying a GFP-marked balancer chromosome. This probably resulted from an unknown balancer chromosome mutation. Thus, we tested whether a mutant *zip* allele also dominantly enhances the *baz* mutant phenotype by generating double heterozygote females and crossing them with wild-type males (Fig. 7A). In contrast to zygotic *baz* mutants alone, which had no AJ phenotype (0/90 embryos), 17/86 of the progeny of the double heterozygote females displayed AJ defects (approximately the expected Mendelian ratio). At stage 8, DE-Cad formed abnormal small puncta along AP contacts (Fig. 7B,C arrowheads) and abnormal larger clusters at DV contacts (Fig. 7B, arrows), contrasting with wild type (Fig. 7F, Fig. 1G). Similarly, stage 10 embryos displayed small DE-Cad puncta (Fig. 7D,E, arrowheads) and abnormal DE-Cad clusters (Fig. 7D, arrows), in contrast to wild type (Fig. 7F). Small puncta were apparent at all elongated contacts observed (enhanced images: Fig. 7C,E). Twenty-five out of 28 isolated large DE-Cad clusters were at non-elongated contacts (eight stage 8-10 embryos counted). In addition, the effects were relatively specific for AS cells, as only 3/17 of the embryos with AS defects displayed AJ defects in other tissues. Thus, Myosin II and Baz function together to coordinate AJ positioning at AP and DV contacts during AS morphogenesis. However, Myosin II and Baz probably act at different contact sites and other players are

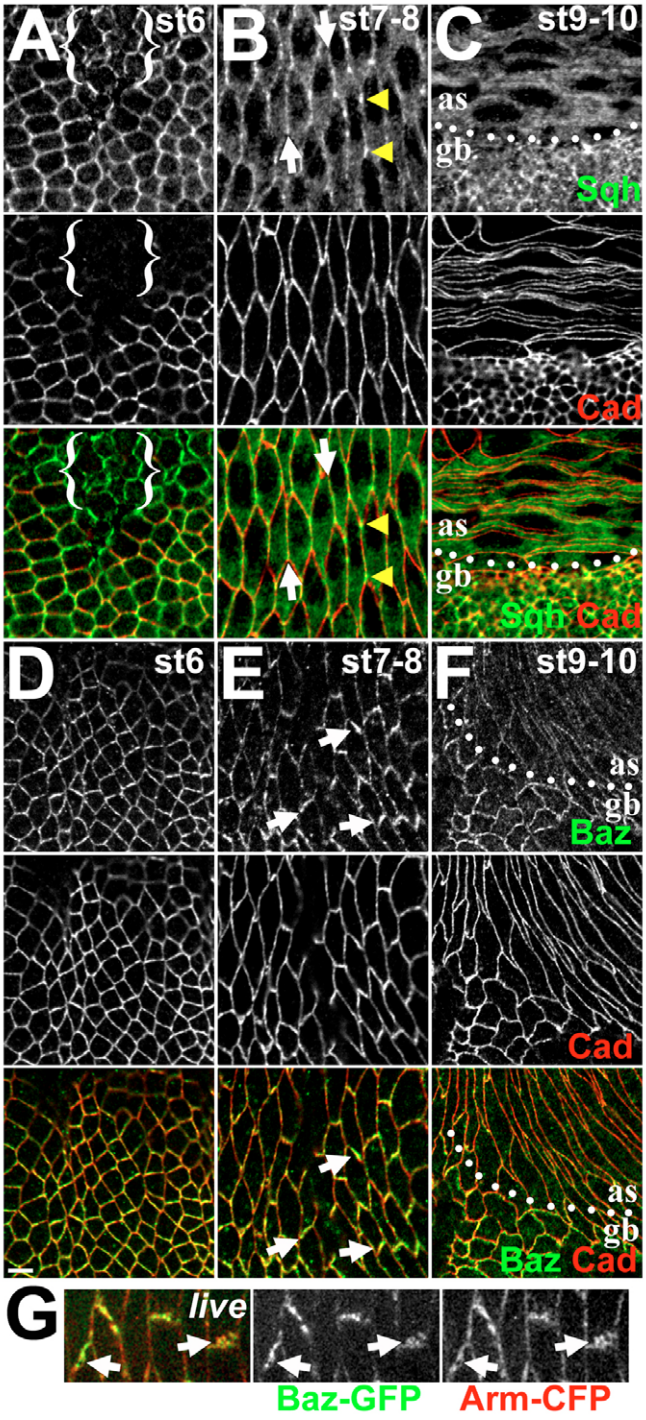

Fig. 6. Myosin II and Bazooka planar polarization during amnioserosa extension. (**A-C**) DE-Cad (red), GFP (green). Sqh-GFP embryos. (A) Stage 6. Sqh localizes at AJs and above (bracketed). (B) Stage 7-8. Sqh localizes along AP contacts (arrows) and at contact ends (arrowheads). (C) Stage 9-10. (**D-F**) DE-Cad (red). Baz (green). Wild-type embryos. (D) Stage 6. Baz colocalizes with DE-Cad. (E) Stage 7-8, DV Baz enrichment (arrows). (F) Stage 9-10. (**G**) Stage 7-8. Live. DV Baz-GFP enrichment and partial colocalization with Arm-CFP looping (arrows) occurs. Scale bar: 5 μm.

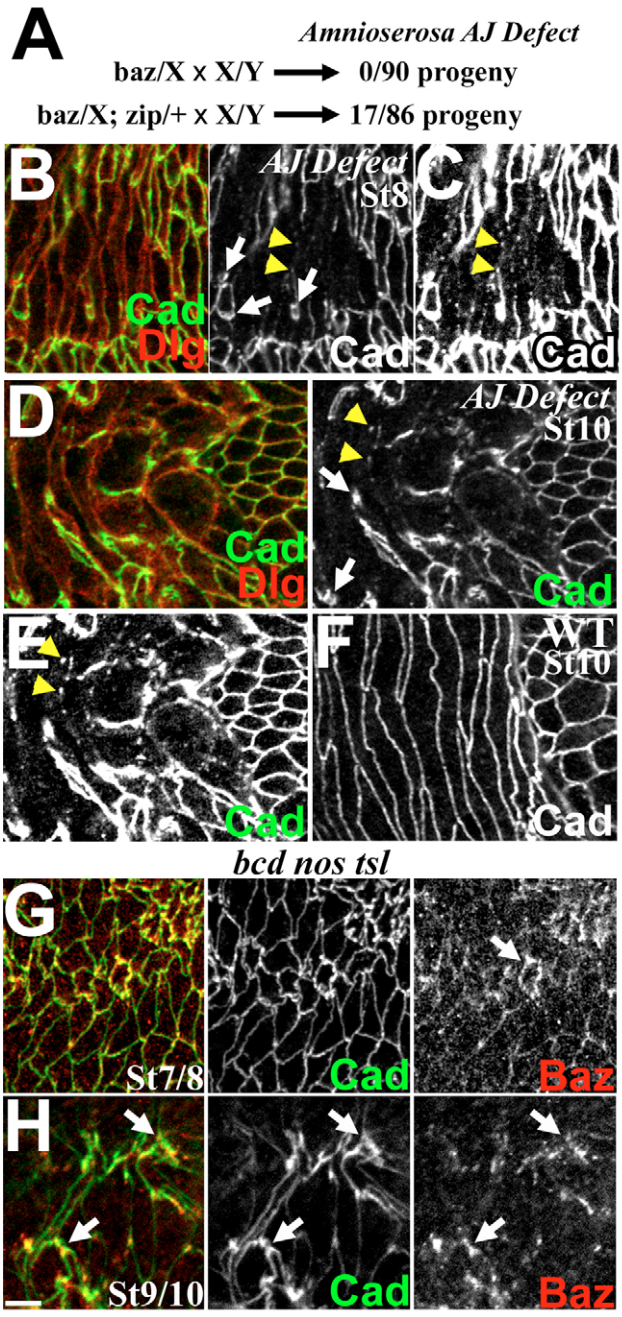

Fig. 7. Bazooka and Myosin II synergy during amnioserosa AJ remodeling. (**A**) *zipper* heterozygosity enhances *baz* AS AJ phenotype. (**B**) Stage 8 AJ defect. DE-Cad puncta (arrowheads), large clusters (arrows). Dlg (red). (**C**) Enhanced DE-Cad image in B. (**D**) Stage 10 AJ defect. DE-Cad (green) puncta (arrowheads) and large clusters (arrows). Dlg (red). (**E**) Enhanced DE-Cad image in D. (**F**) Stage 10 wild type. (**G**,**H**) *bcd nos tsl* mutants. (G) Stage 7-8. DE-Cad (green). Baz (red) planar polarity is abnormal or absent (arrow). (H) Stage 10. DE-Cad (green) clustering (arrows). Baz (red). Scale bar: 5 μm.

undoubtedly involved. Implicating AP patterning, stage 7-8 *bcd nos tsl* mutants displayed no or abnormal Baz planar polarity (Fig. 7G, arrow) and stage 9-11 *bcd nos tsl* mutants displayed abnormal DE-Cad clustering at non-elongated contacts colocalized with abnormally persistent Baz accumulations (compare Fig. 7H, arrows with Fig. 6F).

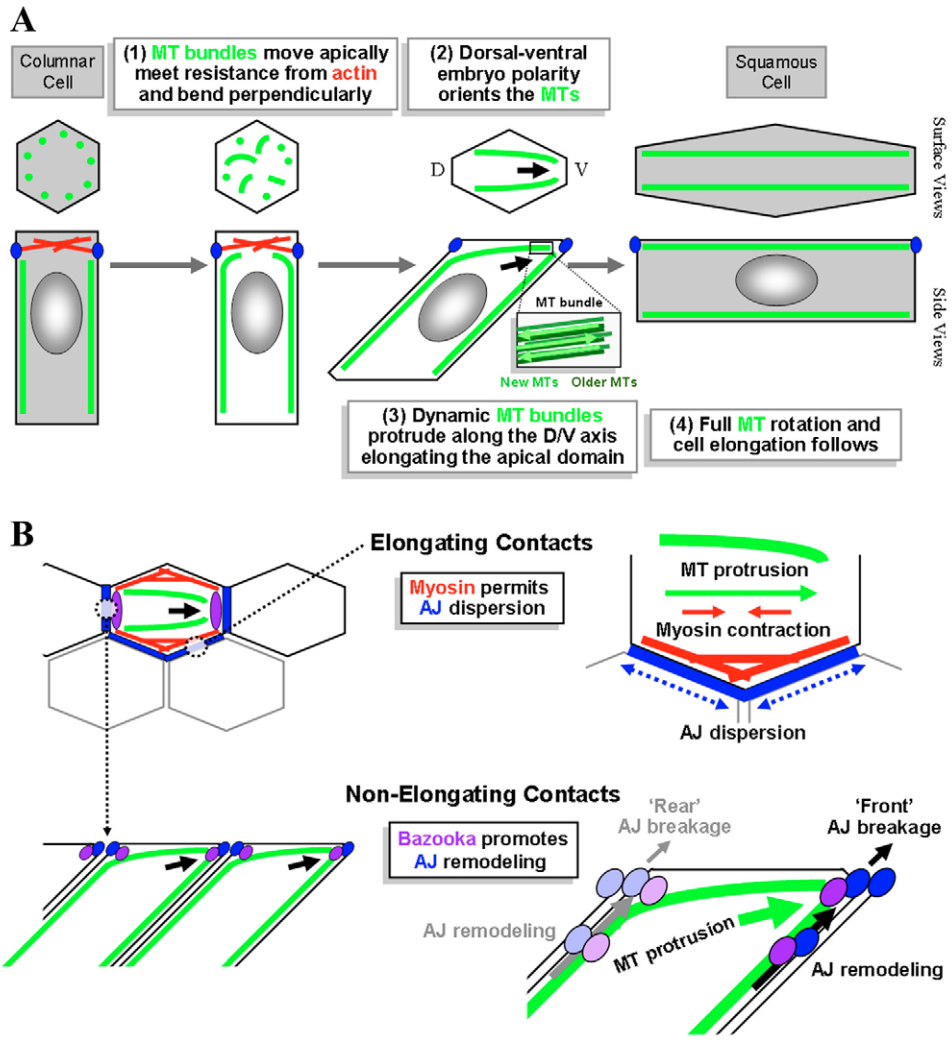

Fig. 8. Models of tissue extension by rotary cell elongation. (**A**) A model of amnioserosa rotary cell elongation. (**B**) A model of amnioserosa junctional remodeling.

DISCUSSION

AS tissue morphogenesis involves dramatic cell shape change. Before AS morphogenesis, cells are columnar with lateral MT bundles in a basket-like array along the apicobasal axis (Harris and Peifer, 2007; Warn and Warn, 1986). With AS morphogenesis, the cells elongate and flatten. AS cells could change shape by symmetrically re-positioning cellular contents (full cytoskeleton and/or membrane reorganization) or by perpendicularly rotating cellular components to reorient the long axis of the cell into the plane of tissue extension. To distinguish these possibilities, we analyzed 3D cell organization over time and discovered that the MT array plus the nucleus, centrosomes and ER rotate, apparently as a unit, into the plane of tissue extension – we term this 'rotary cell elongation' (Fig. 2). As discussed below, more symmetric AJ and cortical reorganizations appear to accompany the rotation. MT arrays also reorient to polarize cells during chemotaxis and tissue migration (Siegrist and Doe, 2007), and to reposition cell contents as occurs during cortical rotation in early *Xenopus* embryos (Weaver and Kimelman, 2004). Our results reveal rotation of the MT cytoskeleton linked to cell shape change and AS morphogenesis. Similar mechanisms may underlie the development of other squamous epithelial monolayers.

Cytoskeletal control of rotary cell elongation

Regulated apical MT protrusion appears to initiate AS rotary cell elongation (model in Fig. 8A). MT inhibition perturbs initial elongation, and the process normally begins with MTs protruding into the apical domain, bending perpendicularly and then extending in the axis of cell elongation. Pre-existing lateral MT bundles appear to protrude across the apical domain – they are mainly non-centrosomal and contain older (acetylated) MTs. However, our EB1-GFP imaging also revealed bi-directional MT growth across the apical domain. This indicates that the bundles are dynamic, but argues against MT bundle protrusion through polarized individual MT polymerization. Instead, MT bundle protrusion may involve greater net renewal of bundles apically versus basally, motors sliding MTs past MTs in the bundles and/or motors moving bundles along the cell cortex. Distinguishing these models requires further study.

As MTs extend apically the actin cytoskeleton appears to inhibit them, as weakening actin leads to excessively long and randomly oriented MT-based protrusions. Actin is normally found around the full apical circumference as AS cells elongate (Figs 1 and 2). By contrast, Myosin II becomes enriched at AP contacts and is gradually lost from the full cell cortex (Fig. 5) (Bertet et al., 2004). Thus, different pools of actin may regulate MT protrusion. We

speculate that the gradual overall loss of cortical actin-myosin complexes permits, and may help orient, regulated MT protrusion (Fig. 8A). Actin also antagonizes cortical MTs in other systems. MT-based primary axons form where cortical actin is weakest (Bradke and Dotti, 1999). Actin inhibits cortical MT protrusion in neutrophils (Eddy et al., 2002) and Myosin IIA inhibits cortical MTs in mammalian cells (Even-Ram et al., 2007). Actin might physically block MT protrusion, but direct or indirect molecular interactions may also be involved (Etienne-Manneville, 2004; Rodriguez et al., 2003).

In *Drosophila* embryos, MT-actin interactions also affect germband cells. At stage 7-8, actin disruption enhances AJ planar polarity at DV contacts (Harris and Peifer, 2007). MT disruption suppresses this, suggesting that actin inhibits MT-based AJ positioning in these cells – however, germband cells show minimal shape change with actin disruption at this stage (Harris and Peifer, 2007). Remarkably, the same actin disruption causes stage 9-10 germband cells to rotate analogously to early AS cells. Their apical domains elongate and their lateral regions rotate perpendicularly, becoming exposed to the embryo surface. Implicating MTs in this change, lateral MT bundles run into the extended apical domains and simultaneous MT disruption suppresses the cell shape change. Thus, actin may inhibit apical MTs to regulate tissue structure in many parts of the embryo. This MT inhibition may also involve coordination with AJs, as disrupted germband cells in *arm*$^{m/z}$ mutants also display MTs protruding into extended apical domains (Harris and Peifer, 2004).

How do MTs elongate the apical domain and how is this linked to the rotation of the full MT cytoskeleton in the AS? We propose that rotary cell elongation occurs in two phases. In phase one, our MT imaging and inhibitor studies indicate that regulated MT protrusion elongates the apical domain. This may involve a combination of physical force, membrane delivery and/or relaxation of actin-myosin contractility (Etienne-Manneville, 2004). The AJ clustering we observed at abnormal apical MT protrusions formed with actin inhibition in both early AS cells and the later germband suggests that MTs may apply force to AJs. Consistent with this idea, MT inhibition affected both initial AS cell elongation and later AS cell-cell interactions (Fig. 3E-H). However, AS cell elongation in *arm*$^{m/z}$ mutants suggests that MTs may not necessarily engage AJs directly. As Baz localizes apically in early *arm*$^{m/z}$ mutants (Harris and Peifer, 2004), and is enriched at DV AS cell contacts to which MTs rotate in wild type, it is a strong candidate for coordinating these interactions. However, severe early defects in *baz*$^{m/z}$ mutants (Harris and Peifer, 2004; Muller and Wieschaus, 1996) would confound analysis of AS development – this may require conditional mutants. Phase two of rotary cell elongation requires full perpendicular rotation of the MT array, apical and basal membrane growth, and lateral membrane removal. Although it is unclear how full rotation occurs, MT rotation and cortical remodeling may occur in concert. For example, membrane remodeling may explain how AS cells remain elongated with MT disruption during later development (Fig. 3E-H).

Planar polarity and AJ remodeling during rotary cell elongation

For rotary cell elongation to translate into tissue extension, cell contacts and AJs must be remodeled. Remarkably, AS cells maintain their neighbor relationships as they elongate, and two contact types develop; highly elongated AP contacts and lesser elongated DV contacts. Each appears to involve unique AJ remodeling. Intriguingly, Myosin II and Baz localize to AP and DV contacts, respectively – the same reciprocal planar polarized relationship displayed in the germband (Bertet et al., 2004; Zallen and Wieschaus, 2004). In the AS, Myosin II and Baz synergize to control overall AJ positioning, a regulatory interaction that, to our knowledge, has not been shown elsewhere.

Myosin II and Baz may regulate specific AJ remodeling events occurring at AP and DV contacts, respectively (see model in Fig. 8B). AS cells increase their apical circumference ~10-fold, initially doubling the length of their AP cell contacts every 5-10 minutes. Remarkably, AJs localize around the full circumference as this occurs. This contrasts elongating *Drosophila* follicle cells, which lose AJ continuity (Grammont, 2007), suggesting specific mechanisms for maintaining AJ continuity during AS morphogenesis. AS AJs do lose continuity with actin disruption, suggesting a role for actin. More specifically, AJ fragmentation in *baz zip* double mutants suggests a role for Myosin II. In the neighboring ventral furrow and germband, actin-myosin contractility is coupled to AJs during apical constriction (Dawes-Hoang et al., 2005) and cell intercalation (Bertet et al., 2004), respectively. The actin-myosin complexes enriched along AS AP contacts may also be contractile, but here they may counterbalance MT protrusion (Fig. 8B). Slowing apical elongation may indirectly allow AJ remodeling. However, Myosin II may also have direct affects on AJs, as evident in *Drosophila* (Bertet et al., 2004; Dawes-Hoang et al., 2005) and elsewhere (Ivanov et al., 2007; Miyake et al., 2006; Shewan et al., 2005; Yamada and Nelson, 2007).

Baz may regulate distinct AJ re-modeling at DV contacts. We hypothesize that MT protrusion applies force to the DV contact at the cell 'front', and that cell elongation may also pull the 'rear' contact (Fig. 8B). Either force could detach AJs and necessitate AJ remodeling. We observed dynamic looping of DE-CadGFP and ArmCFP at D-V contacts, and BazGFP partly colocalized with these loops. Although further experiments (e.g. photobleaching) are needed to understand this and other AS AJ remodeling, Baz localization at DV contacts and abnormal AJ aggregation at DV contacts in *baz zip* double mutants suggests a role for Baz in AJ remodeling at these sites. Baz appears to interact with MTs and Dynein to initially position AJs during *Drosophila* cellularization (Harris and Peifer, 2005), and Baz might re-position AJs at DV AS contacts in a similar way (Fig. 8B).

Orienting rotary cell elongation

In four different cases, we observed cells elongating towards potential sources of pulling forces. First, wild-type AS cells elongate along the DV axis towards the germband (potential source of DV pulling forces during convergent extension) and the ventral furrow (potential source of DV pulling forces during invagination). Second, AS cells elongate along the DV axis of *bcd nos tsl* mutants (Fig. 1S,Y), in which germband extension fails (Irvine and Wieschaus, 1994), but ventral furrow formation occurs. Third, in *dl* mutants in which the ventral furrow does not form and the AS forms a ring around the DV axis (Ray et al., 1991), AS cells reoriented along the AP axis towards ectopic contractile furrows (Fig. 1X,Y). Fourth, in the stage 9-11 wild-type germband, cells artificially induced to flatten and elongate did so in coordinated groups oriented towards contractile regions of the germband (Fig. 4I,J). Thus, polarized pulling forces across a tissue may orient rotary cell elongation. In wild-type embryos, these forces may come from germband extension and/or ventral furrow formation. However, Zen must first trigger the AS cell shape change (Fig. 8A), while AP patterning may specifically regulate AJ remodeling (Fig. 8B).

We thank D. Godt, U. Tepass and R. Winklbauer for critiques. We thank R. Karess, H. Ohkura, M. Peifer, E. Wieschaus, A. Wilde, A. Wodarz, the BDSC and the DSHB for reagents. Work supported by a CIHR operating grant. T.H. holds a Canada Research Chair.

Supplementary material

Supplementary material for this article is available at http://dev.biologists.org/cgi/content/full/135/13/2227/DC1

References

Arora, K. and Nusslein-Volhard, C. (1992). Altered mitotic domains reveal fate map changes in Drosophila embryos mutant for zygotic dorsoventral patterning genes. *Development* **114**, 1003-1024.

Bertet, C., Sulak, L. and Lecuit, T. (2004). Myosin-dependent junction remodelling controls planar cell intercalation and axis elongation. *Nature* **429**, 667-671.

Blankenship, J. T., Backovic, S. T., Sanny, J. S., Weitz, O. and Zallen, J. A. (2006). Multicellular rosette formation links planar cell polarity to tissue morphogenesis. *Dev. Cell* **11**, 459-470.

Bradke, F. and Dotti, C. G. (1999). The role of local actin instability in axon formation. *Science* **283**, 1931-1934.

Cox, R. T., Kirkpatrick, C. and Peifer, M. (1996). Armadillo is required for adherens junction assembly, cell polarity, and morphogenesis during Drosophila embryogenesis. *J. Cell Biol.* **134**, 133-148.

Dawes-Hoang, R. E., Parmar, K. M., Christiansen, A. E., Phelps, C. B., Brand, A. H. and Wieschaus, E. F. (2005). *folded gastrulation*, cell shape change and the control of myosin localization. *Development* **132**, 4165-4178.

Eddy, R. J., Pierini, L. M. and Maxfield, F. R. (2002). Microtubule asymmetry during neutrophil polarization and migration. *Mol. Biol. Cell* **13**, 4470-4483.

Etienne-Manneville, S. (2004). Actin and microtubules in cell motility: which one is in control? *Traffic* **5**, 470-477.

Even-Ram, S., Doyle, A. D., Conti, M. A., Matsumoto, K., Adelstein, R. S. and Yamada, K. M. (2007). Myosin IIA regulates cell motility and actomyosin-microtubule crosstalk. *Nat. Cell Biol.* **9**, 299-309.

Gibson, M. C. and Schubiger, G. (2001). Drosophila peripodial cells, more than meets the eye? *BioEssays* **23**, 691-697.

Grammont, M. (2007). Adherens junction remodeling by the Notch pathway in Drosophila melanogaster oogenesis. *J. Cell Biol.* **177**, 139-150.

Grevengoed, E. E., Fox, D. T., Gates, J. and Peifer, M. (2003). Balancing different types of actin polymerization at distinct sites: roles for Abelson kinase and Enabled. *J. Cell Biol.* **163**, 1267-1279.

Grieder, N. C., de Cuevas, M. and Spradling, A. C. (2000). The fusome organizes the microtubule network during oocyte differentiation in Drosophila. *Development* **127**, 4253-4264.

Harris, T. J. and Peifer, M. (2004). Adherens junction-dependent and -independent steps in the establishment of epithelial cell polarity in Drosophila. *J. Cell Biol.* **167**, 135-147.

Harris, T. J. and Peifer, M. (2005). The positioning and segregation of apical cues during epithelial polarity establishment in Drosophila. *J. Cell Biol.* **170**, 813-823.

Harris, T. J. and Peifer, M. (2007). aPKC controls microtubule organization to balance adherens junction symmetry and planar polarity during development. *Dev. Cell* **12**, 727-738.

Irvine, K. D. and Wieschaus, E. (1994). Cell intercalation during Drosophila germband extension and its regulation by pair-rule segmentation genes. *Development* **120**, 827-841.

Ivanov, A. I., Bachar, M., Babbin, B. A., Adelstein, R. S., Nusrat, A. and Parkos, C. A. (2007). A unique role for nonmuscle myosin heavy chain IIA in regulation of epithelial apical junctions. *PLoS ONE* **2**, e658.

Jacinto, A. and Martin, P. (2001). Morphogenesis: unravelling the cell biology of hole closure. *Curr. Biol.* **11**, R705-R707.

Keller, R., Davidson, L. A. and Shook, D. R. (2003). How we are shaped: the biomechanics of gastrulation. *Differentiation* **71**, 171-205.

Kiehart, D. P., Galbraith, C. G., Edwards, K. A., Rickoll, W. L. and Montague, R. A. (2000). Multiple forces contribute to cell sheet morphogenesis for dorsal closure in Drosophila. *J. Cell Biol.* **149**, 471-490.

Lecuit, T. and Lenne, P. F. (2007). Cell surface mechanics and the control of cell shape, tissue patterns and morphogenesis. *Nat. Rev. Mol. Cell Biol.* **8**, 633-644.

Lee, C., Scherr, H. M. and Wallingford, J. B. (2007). Shroom family proteins regulate gamma-tubulin distribution and microtubule architecture during epithelial cell shape change. *Development* **134**, 1431-1441.

Leptin, M. (1999). Gastrulation in Drosophila: the logic and the cellular mechanisms. *EMBO J.* **18**, 3187-3192.

McCartney, B. M., McEwen, D. G., Grevengoed, E., Maddox, P., Bejsovec, A. and Peifer, M. (2001). Drosophila APC2 and Armadillo participate in tethering mitotic spindles to cortical actin. *Nat. Cell Biol.* **3**, 933-938.

Miyake, Y., Inoue, N., Nishimura, K., Kinoshita, N., Hosoya, H. and Yonemura, S. (2006). Actomyosin tension is required for correct recruitment of adherens junction components and zonula occludens formation. *Exp. Cell Res.* **312**, 1637-1650.

Muller, H. A. and Wieschaus, E. (1996). armadillo, bazooka, and stardust are critical for early stages in formation of the zonula adherens and maintenance of the polarized blastoderm epithelium in Drosophila. *J. Cell Biol.* **134**, 149-163.

O'Connor, M. B., Umulis, D., Othmer, H. G. and Blair, S. S. (2006). Shaping BMP morphogen gradients in the Drosophila embryo and pupal wing. *Development* **133**, 183-193.

Oda, H. and Tsukita, S. (2001). Real-time imaging of cell-cell adherens junctions reveals that Drosophila mesoderm invagination begins with two phases of apical constriction of cells. *J. Cell Sci.* **114**, 493-501.

Oda, H., Uemura, T., Harada, Y., Iwai, Y. and Takeichi, M. (1994). A Drosophila homolog of cadherin associated with armadillo and essential for embryonic cell-cell adhesion. *Dev. Biol.* **165**, 716-726.

Pilot, F., Philippe, J. M., Lemmers, C. and Lecuit, T. (2006). Spatial control of actin organization at adherens junctions by a synaptotagmin-like protein Btsz. *Nature* **442**, 580-584.

Ray, R. P., Arora, K., Nusslein-Volhard, C. and Gelbart, W. M. (1991). The control of cell fate along the dorsal-ventral axis of the Drosophila embryo. *Development* **113**, 35-54.

Rodriguez, O. C., Schaefer, A. W., Mandato, C. A., Forscher, P., Bement, W. M. and Waterman-Storer, C. M. (2003). Conserved microtubule-actin interactions in cell movement and morphogenesis. *Nat. Cell Biol.* **5**, 599-609.

Royou, A., Sullivan, W. and Karess, R. (2002). Cortical recruitment of nonmuscle myosin II in early syncytial Drosophila embryos: its role in nuclear axial expansion and its regulation by Cdc2 activity. *J. Cell Biol.* **158**, 127-137.

Shewan, A. M., Maddugoda, M., Kraemer, A., Stehbens, S. J., Verma, S., Kovacs, E. M. and Yap, A. S. (2005). Myosin 2 is a key Rho kinase target necessary for the local concentration of E-cadherin at cell-cell contacts. *Mol. Biol. Cell* **16**, 4531-4542.

Siegrist, S. E. and Doe, C. Q. (2007). Microtubule-induced cortical cell polarity. *Genes Dev.* **21**, 483-496.

Solnica-Krezel, L. (2006). Gastrulation in zebrafish – all just about adhesion? *Curr. Opin. Genet. Dev.* **16**, 433-441.

Tepass, U. and Hartenstein, V. (1994). The development of cellular junctions in the Drosophila embryo. *Dev. Biol.* **161**, 563-596.

Van Aelst, L. and Symons, M. (2002). Role of Rho family GTPases in epithelial morphogenesis. *Genes Dev.* **16**, 1032-1054.

Warn, R. M. and Warn, A. (1986). Microtubule arrays present during the syncytial and cellular blastoderm stages of the early Drosophila embryo. *Exp. Cell Res.* **163**, 201-210.

Weaver, C. and Kimelman, D. (2004). Move it or lose it: axis specification in Xenopus. *Development* **131**, 3491-3499.

Yamada, S. and Nelson, W. J. (2007). Localized zones of Rho and Rac activities drive initiation and expansion of epithelial cell cell adhesion. *J. Cell Biol.* **178**, 517-527.

Yamanaka, Y., Ralston, A., Stephenson, R. O. and Rossant, J. (2006). Cell and molecular regulation of the mouse blastocyst. *Dev. Dyn.* **235**, 2301-2314.

Zallen, J. A. and Wieschaus, E. (2004). Patterned gene expression directs bipolar planar polarity in Drosophila. *Dev. Cell* **6**, 343-355.